

# Electrocatalysis

# Enhanced Electrocatalytic Activity of a Zinc Porphyrin for CO<sub>2</sub> Reduction: Cooperative Effects of Triazole Units in the Second Coordination Sphere

Amir Lashgari<sup>+</sup>,<sup>[a]</sup> Caroline K. Williams<sup>+</sup>,<sup>[a]</sup> Jenna L. Glover,<sup>[a]</sup> Yueshen Wu,<sup>[b]</sup> Jingchao Chai,<sup>[a]</sup> and Jianbing "Jimmy" Jiang<sup>\*[a]</sup>

**Abstract:** The control of the second coordination sphere in a coordination complex plays an important role in improving catalytic efficiency. Herein, we report a zinc porphyrin complex **ZnPor8T** with multiple flexible triazole units comprising the second coordination sphere, as an electrocatalyst for the highly selective electrochemical reduction of carbon dioxide (CO<sub>2</sub>) to carbon monoxide (CO). This electrocatalyst converted CO<sub>2</sub> to CO with a Faradaic efficiency of 99% and a current density of  $-6.2 \, \text{mA} \, \text{cm}^{-2}$  at  $-2.4 \, \text{V} \, \text{vs. Fc/Fc}^+$  in *N,N*-dimethylformamide using water as the proton source. Struc-

ture-function relationship studies were carried out on **ZnPor8T** analogs containing different numbers of triazole units and distinct triazole geometries; these unveiled that the triazole units function cooperatively to stabilize the CO<sub>2</sub>-catalyst adduct in order to facilitate intramolecular proton transfer. Our findings demonstrate that incorporating triazole units that function in a cooperative manner is a versatile strategy to enhance the activity of electrocatalytic CO<sub>2</sub> conversion.

#### Introduction

The second coordination sphere of a coordination complex structure plays a critical role in many bioinorganic processes, such as carbon dioxide (CO<sub>2</sub>) activation in carbon monoxide (CO) dehydrogenases.<sup>[1]</sup> This knowledge has led to the successful design of molecular catalysts for carbon dioxide reduction, [2] hydrogen evolution reaction, [3] hydrogen oxidation, [4] and water oxidation. [5] Higher coordination sphere in ligands can promote more selective binding of the substrate to the metal center, facilitating proton and electron donation.[3a,6] Common substituents utilized in second coordination sphere coordination complexes include amines, [2b,7] phenols, [2c,8] urea, [9] amides, [10] carboxylic acids, [11] triazoles, [12] and imidazoles. [13] Nitrogen-containing heterocycles, such as imidazole and triazole, can be protonated and further deliver the proton to the proximal substrate, lowering the transition energy for chemical transformation, and thus to enhance reaction kinetics.[12a,14] Most second coordination spheres are rigidly anchored near the catalytic center to enable substrate binding and proton delivery. By contrast, second coordination spheres linked using sp<sup>3</sup> atoms to the primary coordination moiety can adopt several possible geometries in order to accommodate substrate binding, including the nickel phosphine complexes by DuBois et al., [7b,15] iron complexes by Berben et al., [2f,8] and the nickel 1,5-diaza-3,7-diphosphacyclooctane (P2N2) complex by Shaw et al. [16] In addition, the majority of reported transition metalbased coordination complexes are predominantly based on redox-active metal centers and redox-innocent ligands, taking advantage of unfilled *d*-orbitals of transition metals.<sup>[17]</sup> Novel catalysts comprising redox non-innocent ligands with second coordination spheres and redox-innocent metal centers<sup>[18]</sup> can provide new platforms to understand the fundamental processes, discover novel catalytic mechanisms for enhanced activity, and pave the way toward the development of maingroup-element-based catalysis.[18b,c,19]

Electrochemical reduction of CO<sub>2</sub> into products such as carbon monoxide, formate, and methanol is of great interest for sustainable and environmentally friendly processes to create C<sub>1</sub> building blocks.<sup>[20]</sup> Direct electrochemical conversion of CO<sub>2</sub> requires significantly more negative potentials than predicted by the corresponding thermodynamic potentials, since the further transformation of some intermediates is energetically unfavorable.<sup>[21]</sup> Thus, the chemical transformation of CO<sub>2</sub> suffers from high energy input and sluggish reaction kinetics.<sup>[22]</sup> Electrochemical reduction of CO<sub>2</sub> can proceed via two-, four-, six-, eight-, or more electron processes to give CO, formate, formaldehyde, methanol, methane, or C<sub>2</sub> products.<sup>[23]</sup> Some of the standard thermodynamic potentials of the half-re-

[b] Y. Wu Department of Chemistry, Yale University New Haven, Connecticut 06520 (United States)

[+] These authors contributed equally to this work.

 $\sqsubseteq$  Supporting information and the ORCID identification number(s) for the au-

thor(s) of this article can be found under: https://doi.org/10.1002/chem.202002813.

 <sup>[</sup>a] A. Lashgari,\* C. K. Williams,\* J. L. Glover, Dr. J. Chai, Prof. J. ". Jiang Department of Chemistry, University of Cincinnati P.O. Box 210172, Cincinnati, OH 45221 (United States) E-mail: jianbing.jiang@uc.edu



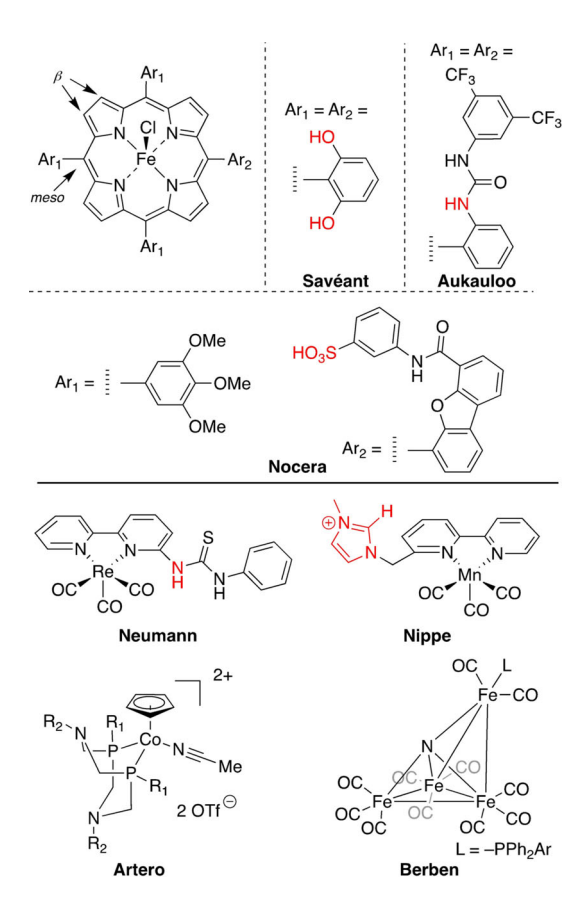
actions of CO<sub>2</sub> reduction are similar, resulting in poor product selectivity.<sup>[20]</sup> Catalysts can lower the transition energy of CO<sub>2</sub> reduction by forming energetically favorable catalyst-CO<sub>2</sub> intermediates, and creating distinct reaction pathways to different products, thus accelerating the reaction rate and improving product selectivity.

Molecular catalysis has gained increasing interest in recent years with the ability to customize catalysts. Through molecular engineering, the solubility, redox potentials, and stability of organic compounds can be readily tuned to explore novel mechanisms and enhance catalytic efficiency. [2a, 24] For example, to increase the redox potential of the catalyst, electron-withdrawing groups, such as nitro and sulfonyl units, can be incorporated in the ligand scaffold of the catalyst. Conversely, the attachment of electron-donating groups, such as alkyl and alkoxy units, to the ligand will decrease the redox potential. [20] Thus, the electron density of the reactive metal ion can be modified.[13b] CO is an attractive chemical feedstock for fuel production because it can be used together with hydrogen gas (as syngas) to synthesize hydrocarbons. [25] Several types of molecular catalysts have proven effective for CO2-to-CO conversion. [26] In particular, metalloporphyrins [26c, 27] have garnered significant attention as efficient molecular catalysts because of (1) efficient synthetic methodologies to prepare the porphyrin framework in one or two steps, [28] (2) the ability to introduce various substituents at the porphyrin meso- and  $\beta$ - positions (Scheme 1), [29] and (3) stable metal complexes resulting from strong binding ability of the four inner nitrogen atoms with various metals.[30] One of the most extensively explored catalyst systems is the iron porphyrin, in which Fe<sup>3+</sup> is electrochemically reduced to Fe<sup>0</sup>, followed by CO<sub>2</sub> binding and conversion (Scheme 1). [2c, 27b] Another highly studied family of molecular catalysts includes bipyridine complexes, since bipyridine ligands can be readily functionalized on the aromatic rings for property tuning, as exemplified by fac-tricarbonyl complexes (Scheme 1).[13a,31] Modification of the ligand scaffold to include a second coordination sphere moiety can improve catalytic efficiency (Scheme 1). Pre-positioned hydrogen donor groups are proposed to stabilize the metal-CO<sub>2</sub> adduct via hydrogen bonding in order to promote intramolecular proton transfer.<sup>[27b, 32]</sup>

Herein, we report the evaluation of a zinc porphyrin complex (**ZnPor8T**) containing second-coordination-sphere triazole units tethered via flexible linkers to the porphyrin core for the electrocatalytic reduction of  $CO_2$  to CO. The **ZnPor8T** catalyst displays excellent activity ( $-6.2~\text{mA}~\text{cm}^{-2}~\text{at}~-2.4~\text{V}~\text{vs}$ . Fc/Fc<sup>+</sup>), high selectivity (CO Faradaic efficiency of 99% at -2.4~V~vs. Fc/Fc<sup>+</sup>), and long-term stability (10 h) for  $CO_2$ -to-CO conversion. The redox properties and catalytic activities of two control compounds (one without the triazole units and another lacking a metal center) were studied for comparison. An extensive investigation was carried out with a set of **ZnPor8T** analogs to elucidate the synergistic effects of the flexible triazole units on electrocatalytic  $CO_2$  reduction. This work represents an example that a flexible second coordination sphere in a molecular catalyst facilitates catalytic  $CO_2$  efficiency. [33]

www.chemeuri.ora

Chem. Eur. J. 2020, 26, 1-9



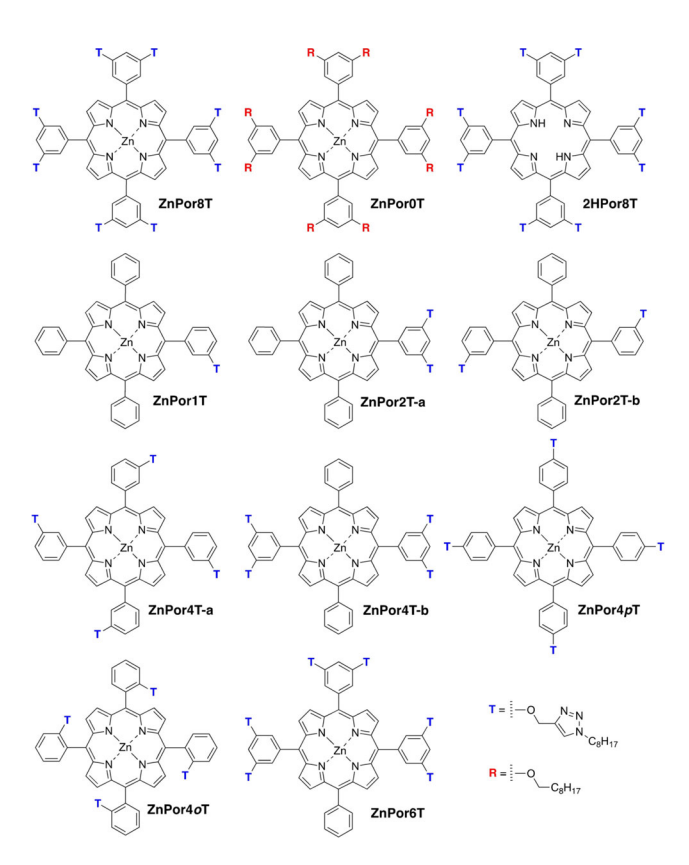
**Scheme 1.** Previously reported complexes that contain a second coordination sphere for hydrogen bonding network formation or proton shuttling.

## **Results and Discussion**

#### Molecular designs and synthesis

A zinc porphyrin complex with eight 1,2,3-triazole units (ZnPor8T) was designed and synthesized (Scheme 2) to investigate the effects of a second coordination sphere comprising flexible triazole groups on electrocatalytic CO<sub>2</sub> reduction. The triazole units are selected because of the strong basicity which enables facile protonation to form hydrogen-bonding network and the straightforward synthesis for the introduction of triazole units via a "click" reaction. Flexible oxymethylene linkers are adopted to connect the triazole units to the porphyrin framework. The non-conjugated oxymethylene linker precludes any possible electronic communication between the second coordination sphere and the porphyrin framework, providing a significant insulating effect. The ZnPor8T catalyst adopts a double-sided picket-fence geometry, providing an identical chemical surface for substrate binding and catalysis on each side of the porphyrin molecular platform. Eight n-octyl chains increase solubility in the reaction medium, N,N-dimethylformamide (DMF), for homogeneous catalysis. A copper(I)-catalyzed alkyne-azide cycloaddition "click" reaction was employed to simultaneously form the triazole units and introduce the alkyl chains. Compounds without the zinc center (2HPor8T) or triazole units (ZnPor0T) were also prepared for control experiments to elucidate the cooperative effects of triazoles.





Scheme 2. Structures of catalysts examined in this work.

Electrocatalyst ZnPor8T was synthesized in a one-step reaction of zinc octaethynylporphyrin (**ZnPor8Y**)<sup>[34]</sup> with 1-azidooctane in the presence of in situ-generated Cu<sup>1</sup> from copper sulfate pentahydrate and sodium ascorbate. The completion of the reaction was tracked by thin layer chromatography during the course of the reaction. Column chromatography was employed to remove trace amounts of impurities to afford a fair reaction yield of 65%. Demetalation of ZnPor8T was achieved using trifluoroacetic acid (TFA) in dichloromethane (CH<sub>2</sub>Cl<sub>2</sub>) to produce 2HPor8T in 95% yield. The control compound ZnPor0T was prepared by zinc metalation of an alkylated freebase porphyrin. All compounds were purified by column chromatography and characterized by proton nuclear magnetic resonance (1H NMR) and matrix-assisted laser desorption/ionization mass spectrometry (see SI for detailed synthesis procedure and Figure S1) prior to any redox and catalysis measurements.

#### **Electrochemical properties**

The electrochemical properties of the **ZnPor8T** electrocatalyst were explored with cyclic voltammetry (CV) with 0.5 mM **ZnPor8T** in DMF containing 0.1 M tetrabutylammonium hexafluorophosphate (TBAPF<sub>6</sub>) under argon atmosphere. The first one-electron reduction with a peak-to-peak separation of 76 mV (at 50 mV s<sup>-1</sup>) and  $i_c/i_a$  of 1.01 (Figure S2) was observed at -1.75 V vs. Fc/Fc<sup>+</sup>, and second reduction occurred at -2.18 V vs. Fc/Fc<sup>+</sup> with almost no corresponding anodic current (Figure 1A). In analogy to previous report, <sup>[26c]</sup> these two redox couples were assigned to porphyrin ligand-based redox

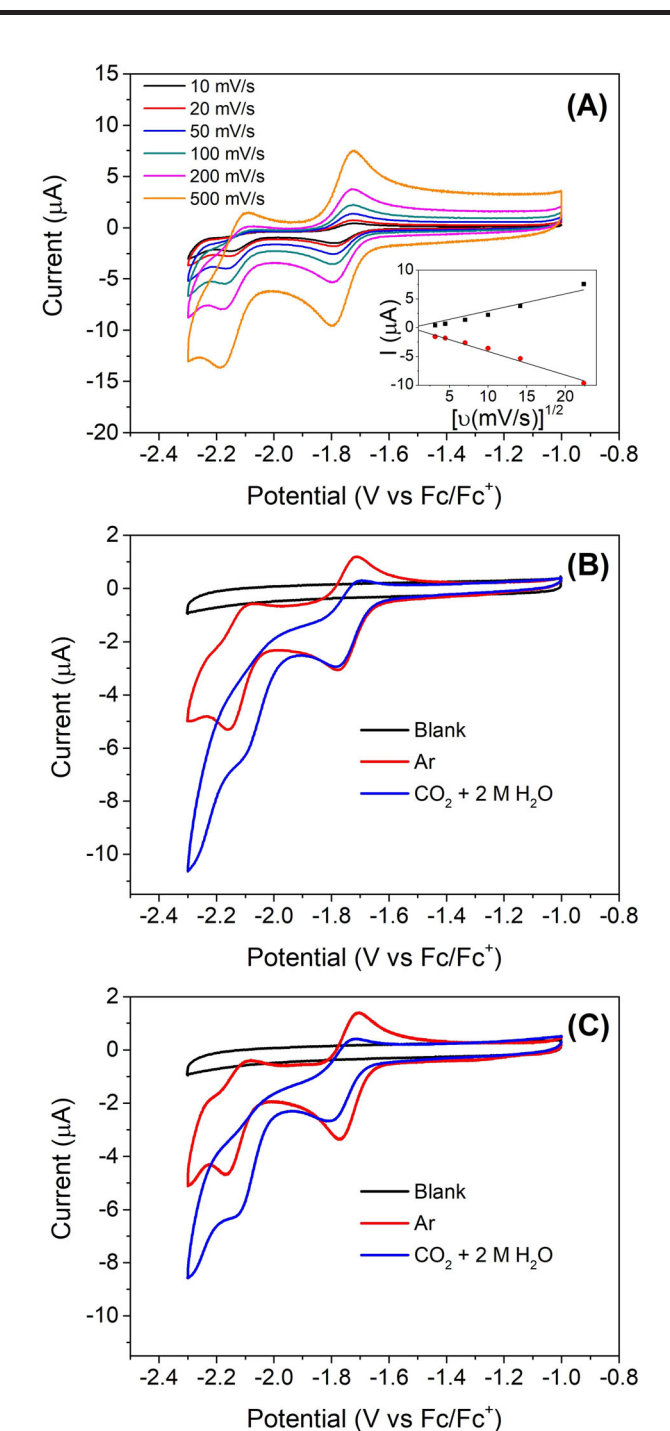


**Figure 1.** (A) Scan-rate dependent CV of 0.5 mM **ZnPor8T** in DMF with 0.1 M TBAPF<sub>6</sub>. Inset: Square root of scan rate vs. current for the first redox peak. CV of (black) a blank solution and 0.5 mM (B) **ZnPor8T** and (C) **ZnPor0T** in DMF/0.1 M TBAPF<sub>6</sub> with (red) Ar and (green) in  $CO_2$  atmosphere with 2 M  $H_2O$  at a scan rate of 50 mV s<sup>-1</sup>.

processes, while the zinc center remained redox innocent. CV was carried out with different scan rates  $(10-500 \text{ mV s}^{-1})$  under the same conditions; the peak current at -1.75 V vs. Fc/Fc<sup>+</sup> was plotted against the square root of the scan rate (Figure 1 A inset). The observed linear trend is indicative of a diffusion-controlled process according to the Randles-Sevcik equation and the absence of obvious deposition of the compound on



the surface of the electrode. [35] Similar redox potentials were observed for the two successive one-electron (Figure 1 C, red trace) reduction processes for the control compound **ZnPor0T** under identical measurement conditions. This confirms that incorporating the triazole units via an oxymethylene linker does not impose significant electronic effects on the zinc porphyrin core.

While CO<sub>2</sub> reduction can occur under aprotic conditions, [36] protonation of the metallocarboxylate intermediate by exogenous proton sources can promote C-O bond cleavage. [13b] A catalytic study was initiated using CV measurements with 0.5 mM ZnPor8T catalyst in DMF/H2O (2 M) with saturated argon or CO<sub>2</sub>. After the electrolyte solution was saturated with CO<sub>2</sub> (0.23 mM)<sup>[2c]</sup> and 2 M H<sub>2</sub>O, a substantial increase in current was observed (Figure 1B) after the one-electron reduction potential with a half-wave potential at -2.1 V vs. Fc/Fc<sup>+</sup>, corresponding to an overpotential of 830 mV (see Supporting Information for calculation).[37] The current increase is attributed to reduction of CO<sub>2</sub> to CO, as verified by controlled potential electrolysis (CPE, vide infra). When hydrated, CO<sub>2</sub> forms H<sub>2</sub>CO<sub>3</sub> (pKa  $\!=\!7.37$  in DMF),  $^{[2a]}$  which functions as the proton source for CO<sub>2</sub> reduction. A S-shape feature of the catalytic wave was not achieved at various scan rates (Figure S3), indicating the absence of pure kinetic condition. [2a,38] The normalized catalytic current  $(i_{cat}/i_{p})$  is related to the maximum turnover frequency (TOF) of the catalytic reaction. Due to the fact that the catalytic CVs of the catalyst are not ideal S-shaped waveforms, foot-ofthe-wave analysis (FOWA) has to be performed (Figure S4). Using Equation (1), the TOF<sub>max</sub> is 222 s<sup>-1</sup>. The normalized current ( $i/i_p$ ) plotted as a function of  $1/\{1 + \exp[(nF/RT)(E-E_{redox})]\}$ achieves the FOWA plot and the slope of the linear portion of the data is used to calculate  $n'k_{\text{obs}}$  which is equal to the  $\mathsf{TOF}_{\mathsf{max}}.^{81}$  The CV of  $\mathsf{ZnPor0T}$  showed two cathodic peaks and current increase in the presence of CO<sub>2</sub> and H<sub>2</sub>O, ascribing to hydrogen evolution (Figure 1C), as confirmed in the following electrolysis studies. Taken together, these results strongly suggest that the pendant triazole units play a critical role in electrocatalytic CO<sub>2</sub> reduction.

$$\frac{i}{i_{\rm p}} = \frac{2.24 \sqrt{\frac{RT}{nFv}} \sqrt{\text{TOF}_{\rm max}}}{1 + \exp\left[\frac{nF}{RT} (E - E_{redox})\right]}$$

where i is the catalytic current,  $i_p$  is the non-catalytic Faradaic current, R is the universal gas constant, T is the temperature, n is the number of electron transfer processes per catalyst, F is the Faraday constant, v is the scan rate, E is the potential, and  $E_{\rm redox}$  is the potential where the catalyst undergoes a mechanistic redox process in the absence of substrate. [39]

To gain insight on electrocatalytic activity, product distribution, and Faradaic efficiency for CO<sub>2</sub> reduction, CPE was performed at various potentials. Carbon fiber paper with a large surface area was used as the working electrode for detectable product generation. On-line gas chromatography was employed to detect gaseous products (Figure S5). At applied potentials more positive than -1.9 V vs. Fc/Fc<sup>+</sup>, hydrogen gas was the only reduction product. As more negative potentials were applied to the working electrode, higher current densities and Faradaic efficiencies were observed, with the highest Faradaic efficiency of 99% for CO and the maximum current density of  $-6.2 \text{ mA cm}^{-2}$  at -2.4 V vs. Fc/Fc<sup>+</sup> (Figure 2 A). Throughout the CPE study, CO and H<sub>2</sub> are the only gaseous reduction products detected. In order to determine whether the triazole group contributes significantly to the high catalytic activity of ZnPor8T, CPE was carried out under the same conditions with the triazole-free control compound ZnPor0T. The maximum current density (-0.6 mA cm<sup>-2</sup>) was one-tenth that observed with ZnPor8T (Figure 2B). To confirm that the blank carbon fiber paper electrode did not catalyze CO<sub>2</sub> conversion, CPE was performed with a catalyst-free electrolyte and a fresh carbon paper electrode (Figure S6). The current density was extremely low  $(-0.25 \text{ mA cm}^{-2})$  during electrolysis; the amount of CO produced was insufficient for precise Faradaic efficiency detection. These results suggest that the triazole groups are mechanistically significant in the selective reduction of CO<sub>2</sub> to CO. Both pre- and post-electrolysis solutions were analyzed using <sup>1</sup>H NMR spectroscopy, and no liquid product was detected, confirming the high selectivity of the ZnPor8T catalyst for CO production (Figure S7). An additional electrolysis was performed using isotopically labeled <sup>13</sup>CO<sub>2</sub> gas and, the post electrolysis solution was analyzed using <sup>13</sup>C NMR spectroscopy, which further confirmed the absence of other CO<sub>2</sub> reduction products (Figure S8). Similarly, the control compound ZnPor0T did not undergo significant destruction of the porphyrin framework or Zn demetalation, according to the <sup>1</sup>H NMR (Fig-

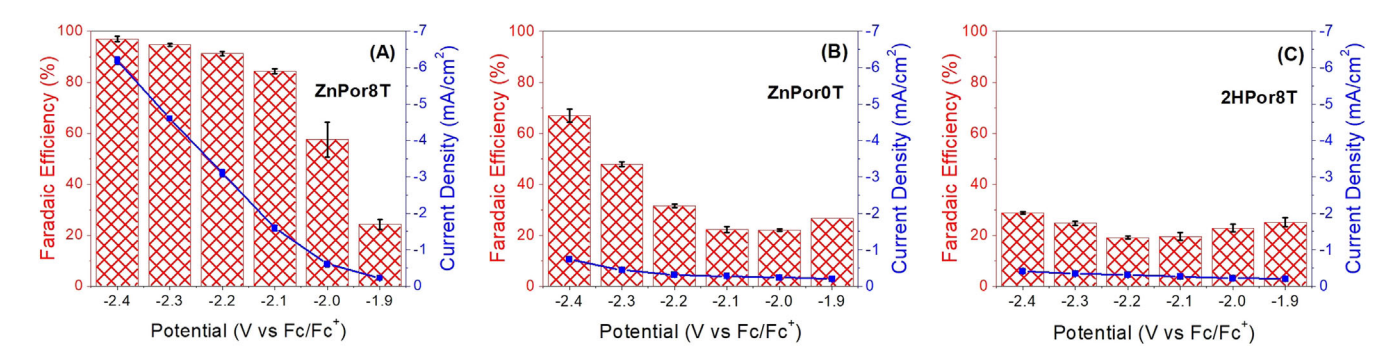


Figure 2. CO Faradaic efficiencies and current densities at various potentials for compounds (A) **ZnPor8T**, (B) **ZnPor0T**, and (C) **2HPor8T**. H<sub>2</sub> gas was the only other product observed.



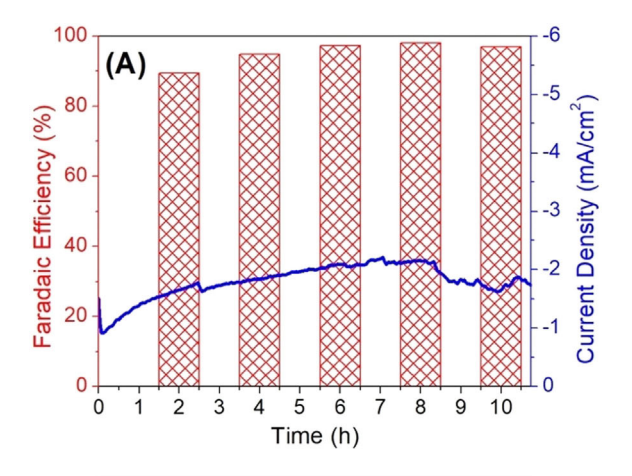
ure S9) and absorption spectroscopy of the post-catalysis solution (Figure S10), ensuring it is a reasonable control compound. The CPE of **ZnPor8T** electrolysis was also performed without  $CO_2$  substrate and hydrogen gas was the only gaseous product detected with a Faradaic efficiency of 20% (Figure S11). A phlorin derivate was also detected via UV/Visible absorption spectroscopy (Figure S12), [18d,40] suggesting porphyrin reduction under the  $CO_2$ -free electrolysis condition.

The metal-free triazole compound 2HPor8T was studied under the same conditions as those used for **ZnPor8T** and ZnPor0T. CPE showed a maximum CO Faradaic efficiency of 28% and a current density of less than -0.5 mA cm<sup>-2</sup> (Figure 2C). Given that elemental zinc is a well-known heterogeneous catalyst for CO<sub>2</sub> reduction,<sup>[41]</sup> a "rinse test" was performed to preclude the possibility that the high activity and selectivity of ZnPor8T resulted from elemental zinc deposited from significant Zn demetalation. The working electrode from the ZnPor8T CPE experiment was soaked in DMF overnight, and then gently rinsed twice with DMF to remove any loosely bound molecular ZnPor8T catalyst. The electrode was then used in a catalyst-free, fresh electrolyte solution to evaluate whether Zn metal had plated onto the carbon paper during the prior experiment. Low current densities (a maximum of  $-0.5 \text{ mA cm}^{-2}$ ) and insignificant CO production (Figure S13) confirmed the absence of any heterogenized ZnPor8T catalyst or elemental zinc on the electrode. The dynamic light scattering measurements of pre- and post-catalysis solution of ZnPor8T showed no detectable particles, further confirming the absence of demetalation during catalysis. [24b] X-ray photoelectron spectroscopy (XPS) showed a small amount of zinc which does not contribute to catalysis according to the negative CPE results of the rinse test (Figure S14).

Long-term bulk electrolysis was performed at  $-2.1 \,\mathrm{V}$  vs. Fc/Fc<sup>+</sup> for 10 h. Faradaic efficiency remained over 90% during electrolysis, with an average current density of  $-1.8 \,\mathrm{mA\,cm^{-2}}$  (Figure 3 A). For additional confirmation of the molecular integrity of the catalyst, UV/Visible absorption spectra of **ZnPor8T** solutions were collected before and after long-term electrolysis. Any free-base porphyrin (derived from demetalation of **ZnPor8T**) can be recognized from the unique spectral features of **2HPor8T** (Figure 3 B, dotted line). No obvious changes to the Q-band region of the spectra were observed, suggesting that this catalyst is a molecular catalyst and did not degrade during electrolysis.

#### Cooperative effects of triazoles

To further investigate the role of the triazole units on catalytic efficiency from a mechanistic standpoint, a set of analogous compounds with different numbers of triazole groups and distinct connection modes were prepared (Scheme 2, see Supporting Information for detailed synthesis), including (1) six compounds with varying numbers (1–6) of triazole groups attached to the *meta*- positions of the phenyl groups of the porphyrin framework (ZnPor1T, ZnPor2T-a, ZnPor2T-b, ZnPor4T-a, ZnPor4T-b, and ZnPor6T), and (2) two compounds with four triazole groups attached to the *para*- (ZnPor4*p*T)



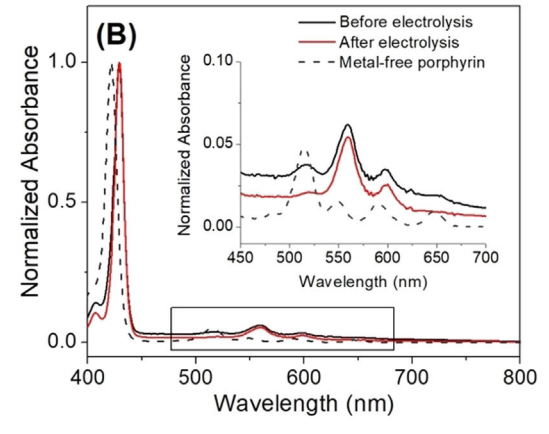


**Figure 3.** (A) CO Faradaic efficiencies and total current densities collected every two hours of the 10 h electrolysis at -2.1 V vs. Fc/Fc $^+$ . Hydrogen gas is the only other reduction product. (B) UV/Visible absorption spectra of the **ZnPor8T** electrolyte solution (black) before and (red) after electrolysis and of the (grey dotted) free-base porphyrin **2HPor8T**. The spectra are normalized in the Soret peak. Inset: expansion of the porphyrin Q-band region.

and *ortho-* (**ZnPor4***o***T**) positions of the phenyl group. Studying catalysis with the various analogs of **ZnPor8T** allows the elucidation of any possible synergistic effects among the triazole groups, as well as geometric effects originating from the connection mode (*ortho* vs. *meta* vs. *para*). The same synthetic strategy was adopted as for the preparation of **ZnPor8T**, which included (1) the formation for porphyrin framework following Lindsey's procedure, [28,42] (2) zinc metalation, and (3) introduction of the triazole units and alkyl tails via a click reaction (See Supporting Information for synthetic details). Each target compound was thoroughly purified and characterized before electrochemical and catalysis analysis.

CPE was performed on the analogs using the same procedure described above. The Faradaic efficiencies and current densities of the triazole catalysts at -2.3 V vs. Fc/Fc $^+$  are listed in Figure 4. Catalysts with one or two triazole units (**ZnPor1T**, **ZnPor2T-a**, and **ZnPor2T-b**) exhibited low activity (maximum current density = 1.0 mA cm $^{-2}$ ) and low selectivity (Figure S17, highest CO Faradaic efficiency  $<60\,\%$ ). Catalysts with a relatively high number (4 or 6) of triazole units (**ZnPor4T-a**, **ZnPor4T-b**, and **ZnPor6T**) displayed higher CO Faradaic efficiencies (70–94% at -2.4 V vs. Fc/Fc $^+$ ), yet still had low current

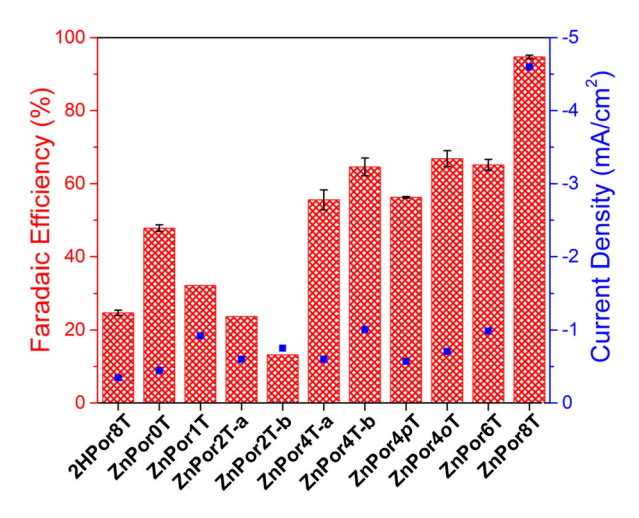


**Figure 4.** Faradaic efficiency (red) and current densities (blue) of the triazole catalysts at -2.3 vs. Fc/Fc<sup>+</sup>.

densities (Figure S17,  $< -1.5 \text{ mA cm}^{-2}$ ). No substantial difference in activity or selectivity was observed between different regioisomers (ZnPor2T-a vs. ZnPor2T-b, ZnPor4T-a vs. ZnPor4T-b, and ZnPor4oT vs. ZnPor4pT). Surprisingly, none of the catalysts displayed comparable activity to ZnPor8T (CO Faradaic efficiency 99% and current density of  $-6.2 \text{ mA cm}^{-2}$ at -2.4 V vs. Fc/Fc<sup>+</sup>). The excellent catalytic performance of **ZnPor8T** does not originate from the sum of the contributions of each individual triazole unit. Rather, the four triazole units on the same side of the **ZnPor8T** porphyrin work cooperatively as a hydrogen-bonding network to enable proton delivery for CO<sub>2</sub> reduction. The limited number of triazoles (0-6) does not construct efficient hydrogen bonding network to facilitate proton transfer from the second coordination sphere to the catalytic center. The zinc center and the surrounding porphyrin ring are the primary coordination sphere (green oval, Figure 5 A). The secondary coordination sphere encompasses are four triazole units on each side of the catalyst, creating a proton rich hydration sphere that enhances CO2 reduction (blue cylinder, Figure 5A). This observation is distinct from that reported for cobalt complexes with various numbers of pendant amines that work noncooperatively for proton transfer. [43] The hydrogen-bonding network formation was observed in the work by Dey et al., where water molecules were trapped in the triazole cavity with triazole units as the hydrogen bonding acceptor.[17f] Through computation on a Mn/bipyridine complex with an imidazole unit, Nippe et al. proposed the existence of two different solvation shells, where the first shell comprises of three water molecules, and the second one contains one water molecule. [13a] The Berben group elucidated the transport mechanisms of proton and CO2 by varying the size of second coordination spheres to allow or inhibit the formation of MeCN-H<sub>2</sub>O adduct.<sup>[2f]</sup> Artero, Fontecave and co-workers proposed solvation effect in a Co/P2N2 complex, which employs one water molecule to bridge the Co/CO<sub>2</sub> adduct and the N atom on the ligand for intermediate stabilization. [2a] In Nocera's work, the appended proton coordinates with the metal/CO<sub>2</sub> adduction for intermediate protonation.<sup>[27b]</sup> DuBois

www.chemeurj.org

Chem. Eur. J. 2020, 26, 1-9

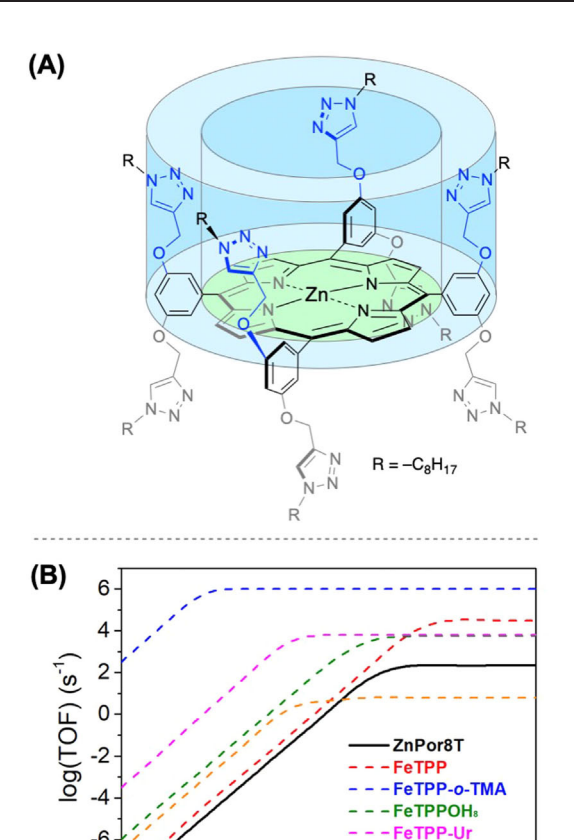


**Figure 5.** (A) Schematic depicting the primary and second coordination spheres of **ZnPor8T**. (B) Tafel plots derived from cyclic voltammograms of **ZnPor8T** in DMF with  $2M\ H_2O$ .

0.4

Overpotential (V)

0.6

0.8

1.0

0.0

0.2

ruthenium complex employs direct coordination of the substrate H<sub>2</sub> with pendant amine for proton transfer.<sup>[4d]</sup>

We attempted to grow single crystals to study the exact positions of the triazole units, but were unsuccessful, presumably due to irregular molecular packing resulting from the multiple alkyl chains. We hypothesize that the four protonated triazole units in ZnPor8T form a hydrophilic picket fence to facilitate proton shuttling to the zinc catalytic center, enhancing activity.[44] In the analogous compounds, due to the lack of sufficient triazole units, each triazole unit behaves individually rather than cooperatively; these do not function as effectively as the triazole bundle in the ZnPor8T catalyst. Similar synergistic effects on CO<sub>2</sub> reduction with multiple proton donors have been observed previously.[2b,9,12a,43] These systems contain second coordination spheres that are prepositioned in close proximity to the catalytic center via rigid anchors to the ligand framework. By contrast, this work represents an example of synergistic effects from a flexible second coordination sphere.

For comparison with several extensively studied iron porphyrin catalysts, <sup>[9]</sup> we plotted our catalysts against five iron porphyrin catalysts (Figure 5 B), including two without a higher coordination sphere (FeTPP<sup>[2e]</sup> and FeTTPF<sub>20</sub><sup>[45]</sup>) and three bearing trimethyl ammonium (FeTPP-o-TMA<sup>[2e]</sup>), hydroxyl (FeTP-



POH<sub>8</sub><sup>[2d]</sup>), and urea (FeTPP-Ur<sup>[9]</sup>) as their second coordination spheres (see Chart S1). In these well studied systems, FeTP-POH<sub>8</sub> utilizes a hydrogen bonding network to transfer protons to the metal center via the hydroxyl groups. Another catalyst, Fe-o-TMA, contains a through-space mechanism by positive charges on the ammonium in the second coordination sphere, which stabilizes the CO<sub>2</sub>-bound intermediate. These second coordination spheres were able to decrease the overpotential from the unsubstituted iron porphyrin, FeTPP. Two methods were adopted to calculate the turnover numbers (TON). The first one takes account of the total amount of CO generated during the 10 h CPE. The  $TON_{CPE}$  is calculated to be 104 (see Supporting Information for calculation details). This method assumes all catalysts in the bulk solution are catalytically active, so the TON<sub>CPE</sub> value only reflects the lower bound of the TON. This value is to be compared to an excellent phthalocyanine catalyst from Robert et al. $^{[46]}$  (TON<sub>CPE</sub> = 29008). The second method entails the extraction of TOF from Tafel plot the -2.1 V vs. Fc/Fc<sup>+</sup> for CPE, termed as TOF<sub>CV</sub>, and the TON<sub>CV</sub> is obtained from the product of  $TOF_{CV}$  and CPE time (10 h). This method only counts the active catalyst in the thin reaction-diffusion layer near the electrode, and reflects the intrinsic activity of the catalyst. The  $TON_{CV}$  is calculated to be  $8.0 \times 10^6$  (see Supporting Information for calculation details), to be compared to an iron porphyrin system from Savéant ( $TOF_{CV} = 6 \times 10^6$ ).<sup>[47]</sup> Although the TON and TOF values of **ZnPor8T** are not comparable with the state-of-the-art electrocatalysts, it demonstrates that **ZnPor8T** is a viable catalyst for CO<sub>2</sub>-to-CO conversion.

### **Conclusions**

A zinc porphyrin molecular catalyst for the reduction of  $CO_2$  to CO has been synthesized with flexible triazole units as the second coordination sphere. The **ZnPor8T** catalyst exhibits a Faradaic efficiency of over 99% with a maximum current density of  $-6.2 \, \text{mA} \, \text{cm}^{-2}$  at  $-2.4 \, \text{V}$  vs. Fc/Fc<sup>+</sup>. This compound was compared to a triazole-free analog, **ZnPor0T**, which exhibited a lower current density and Faradaic efficiency, indicating that the triazole group is mechanistically significant for  $CO_2$  to CO reduction. A series of compounds bearing different numbers of triazole groups and distinct triazole geometries was prepared to study the structure-function relationship. These studies revealed synergistic effects with the triazole groups in **ZnPor8T** for the construction of a hydrogen-bonding network which facilitates the proton transfer step in electrocatalytic  $CO_2$  reduction.

## **Acknowledgements**

The authors acknowledge the University of Cincinnati for startup funding support. NMR experiments were performed on a Bruker AVANCE NEO 400 MHz NMR spectrometer funded by NSF-MRI grant CHE-1726092.

## **Conflict of interest**

The authors declare no conflict of interest.

**Keywords:** carbon-dioxide fixation  $\cdot$  homogeneous catalysis  $\cdot$  porphyrin  $\cdot$  second coordination sphere  $\cdot$  triazole

- [1] J. H. Jeoung, H. Dobbek, Science 2007, 318, 1461 1464.
- a) S. Roy, B. Sharma, J. Pecaut, P. Simon, M. Fontecave, P. D. Tran, E. Derat, V. Artero, J. Am. Chem. Soc. 2017, 139, 3685 3696; b) A. Chapovetsky, T. H. Do, R. Haiges, M. K. Takase, S. C. Marinescu, J. Am. Chem. Soc. 2016, 138, 5765 5768; c) C. Costentin, S. Drouet, M. Robert, J. M. Savéant, Science 2012, 338, 90 94; d) C. Costentin, G. Passard, M. Robert, J. M. Savéant, Proc. Natl. Acad. Sci. USA 2014, 111, 14990–14994; e) I. Azcarate, C. Costentin, M. Robert, J. M. Savéant, J. Am. Chem. Soc. 2016, 138, 16639 16644; f) N. D. Loewen, L. A. Berben, Inorg. Chem. 2019, 58, 16849 16857; g) D. Z. Zee, M. Nippe, A. E. King, C. J. Chanq, J. R. Long, Inorg. Chem. 2020, 59, 5206 5217.
- [3] a) D. L. DuBois, *Inorg. Chem.* 2014, *53*, 3935–3960; b) Q. Liao, T. Liu, S. I. Johnson, C. M. Klug, E. S. Wiedner, R. Morris Bullock, D. L. DuBois, *Dalton Trans.* 2019, *48*, 4867–4878; c) M. Fang, E. S. Wiedner, W. G. Dougherty, W. S. Kassel, T. Liu, D. L. DuBois, R. M. Bullock, *Organometallics* 2014, *33*, 5820–5833.
- [4] a) B. Ginovska-Pangovska, A. Dutta, M. L. Reback, J. C. Linehan, W. J. Shaw, Acc. Chem. Res. 2014, 47, 2621–2630; b) A. Dutta, B. Ginovska, S. Raugei, J. A. Roberts, W. J. Shaw, Dalton Trans. 2016, 45, 9786–9793; c) A. Dutta, S. Lense, J. A. S. Roberts, M. L. Helm, W. J. Shaw, Eur. J. Inorg. Chem. 2015, 5218–5225; d) T. Liu, M. R. DuBois, D. L. DuBois, R. M. Bullock, Energy Environ. Sci. 2014, 7, 3630–3639.
- [5] a) D. W. Shaffer, Y. Xie, D. J. Szalda, J. J. Concepcion, J. Am. Chem. Soc.
  2017, 139, 15347-15355; b) N. Vereshchuk, R. Matheu, J. Benet Buchholz, M. Pipelier, J. Lebreton, D. Dubreuil, A. Tessier, C. Gimbert-Surinach, M. Z. Ertem, A. Llobet, J. Am. Chem. Soc. 2020, 142, 5068-5077; c) W. A. Hoffert, M. T. Mock, A. M. Appel, J. Y. Yang, Eur. J. Inorg. Chem.
  2013, 3846-3857; d) J. F. Khosrowabadi Kotyk, C. M. Hanna, R. L. Combs, J. W. Ziller, J. Y. Yang, Chem. Sci. 2018, 9, 2750-2755.
- [6] J. M. Barlow, J. Y. Yang, ACS Cent. Sci. 2019, 5, 580 588.
- [7] a) L. Kohler, J. Niklas, R. C. Johnson, M. Zeller, O. G. Poluektov, K. L. Mulfort, *Inorg. Chem.* 2019, 58, 1697 1709; b) M. L. Helm, M. P. Stewart, R. M. Bullock, M. R. DuBois, D. L. DuBois, *Science* 2011, 333, 863 866.
- [8] J. Agarwal, T. W. Shaw, H. F. Schaefer III, A. B. Bocarsly, *Inorg. Chem.* 2015, 54, 5285 – 5294.
- [9] P. Gotico, B. Boitrel, R. Guillot, M. Sircoglou, A. Quaranta, Z. Halime, W. Leibl, A. Aukauloo, Angew. Chem. Int. Ed. 2019, 58, 4504–4509; Angew. Chem. 2019, 131, 4552–4557.
- [10] E. M. Nichols, J. S. Derrick, S. K. Nistanaki, P. T. Smith, C. J. Chang, Chem. Sci. 2018, 9, 2952 – 2960.
- [11] a) J. Rosenthal, D. G. Nocera, Acc. Chem. Res. 2007, 40, 543-553; b) C. T. Carver, B. D. Matson, J. M. Mayer, J. Am. Chem. Soc. 2012, 134, 5444-5447.
- [12] a) B. Mondal, A. Rana, P. Sen, A. Dey, J. Am. Chem. Soc. 2015, 137, 11214–11217; b) S. Samanta, K. Sengupta, K. Mittra, S. Bandyopadhyay, A. Dey, Chem. Commun. 2012, 48, 7631–7633; c) B. Mondal, P. Sen, A. Rana, D. Saha, P. Das, A. Dey, ACS Catal. 2019, 9, 3895–3899; d) C. K. Williams, A. Lashgari, J. Chai, J. Jiang, ChemSusChem 2020, 13, 3412–3417.
- [13] a) S. Sung, X. Li, L. M. Wolf, J. R. Meeder, N. S. Bhuvanesh, K. A. Grice, J. A. Panetier, M. Nippe, J. Am. Chem. Soc. 2019, 141, 6569 – 6582; b) S. Sung, D. Kumar, M. Gil-Sepulcre, M. Nippe, J. Am. Chem. Soc. 2017, 139, 13993 – 13996.
- [14] A. Rana, B. Mondal, P. Sen, S. Dey, A. Dey, Inorg. Chem. 2017, 56, 1783 1793.
- [15] A. D. Wilson, R. K. Shoemaker, A. Miedaner, J. T. Muckerman, D. L. DuBois, M. R. DuBois, Proc. Natl. Acad. Sci. USA 2007, 104, 6951–6956.
- [16] See of reference [4c]
- [17] a) E. Tayyebi, J. Hussain, Y. Abghoui, E. Skúlason, J. Phys. Chem. C 2018, 122, 10078 – 10087; b) M. Bourrez, F. Molton, S. Chardon-Noblat, A. Deronzier, Angew. Chem. Int. Ed. 2011, 50, 9903 – 9906; Angew. Chem. 2011,



- 123, 10077–10080; c) T. R. O'Toole, L. D. Margerum, T. D. Westmoreland, W. J. Vining, R. W. Murray, T. J. Meyer, J. Chem. Soc. Chem. Commun. 1985, 1416–1417; d) J. Hawecker, J.-M. Lehn, R. Ziessel, J. Chem. Soc. Chem. Commun. 1984, 328–330; e) A. Singha, K. Mittra, A. Dey, Dalton Trans. 2019, 48, 7179–7186; f) P. Sen, B. Mondal, D. Saha, A. Rana, A. Dey, Dalton Trans. 2019, 48, 5965–5977; g) E. M. Nichols, C. J. Chang, Organometallics 2019, 38, 1213–1218; h) C. Jiang, A. W. Nichols, C. W. Machan. Dalton Trans. 2019, 48, 9454–9468.
- [18] a) O. R. Luca, R. H. Crabtree, Chem. Soc. Rev. 2013, 42, 1440-1459;
  b) A. Z. Haddad, D. Kumar, K. Ouch Sampson, A. M. Matzner, M. S. Mashuta, C. A. Grapperhaus, J. Am. Chem. Soc. 2015, 137, 9238-9241;
  c) E. J. Thompson, L. A. Berben, Angew. Chem. Int. Ed. 2015, 54, 11642-11646; Angew. Chem. 2015, 127, 11808-11812; d) B. H. Solis, A. G. Maher, D. K. Dogutan, D. G. Nocera, S. Hammes-Schiffer, Proc. Natl. Acad. Sci. USA 2016, 113, 485-492.
- [19] E. M. Leitao, T. Jurca, I. Manners, Nat. Chem. 2013, 5, 817-829.
- [20] R. Francke, B. Schille, M. Roemelt, Chem. Rev. 2018, 118, 4631 4701.
- [21] a) B. J. McNicholas, J. D. Blakemore, A. B. Chang, C. M. Bates, W. W. Kramer, R. H. Grubbs, H. B. Gray, J. Am. Chem. Soc. 2016, 138, 11160–11163; b) C. I. Shaughnessy, D. J. Sconyers, T. A. Kerr, H. J. Lee, B. Subramaniam, K. C. Leonard, J. D. Blakemore, ChemSusChem 2019, 12, 3761–3768; c) A. M. Appel, J. E. Bercaw, A. B. Bocarsly, H. Dobbek, D. L. DuBois, M. Dupuis, J. G. Ferry, E. Fujita, R. Hille, P. J. Kenis, C. A. Kerfeld, R. H. Morris, C. H. Peden, A. R. Portis, S. W. Ragsdale, T. B. Rauchfuss, J. N. Reek, L. C. Seefeldt, R. K. Thauer, G. L. Waldrop, Chem. Rev. 2013, 113, 6621–6658.
- [22] P. Kang, Z. Chen, M. Brookhart, T. J. Meyer, *Top. Catal.* **2015**, *58*, 30–45.
- [23] J. Qiao, Y. Liu, F. Hong, J. Zhang, Chem. Soc. Rev. 2014, 43, 631–675.
- [24] a) A. W. Nichols, C. W. Machan, Front. Chem. 2019, 7, 397; b) N. Kaeffer, A. Morozan, J. Fize, E. Martinez, L. Guetaz, V. Artero, ACS Catal. 2016, 6, 3727 3737; c) M. Yousif, A. C. Cabelof, P. D. Martin, R. L. Lord, S. Groysman, Dalton Trans. 2016, 45, 9794 9804; d) R. Narayanan, M. McKinnon, B. R. Reed, K. T. Ngo, S. Groysman, J. Rochford, Dalton Trans. 2016, 45, 15285 15289.
- [25] A. Goeppert, M. Czaun, J. P. Jones, G. K. Surya Prakash, G. A. Olah, Chem. Soc. Rev. 2014, 43, 7995 – 8048.
- [26] a) S. L. Hooe, J. M. Dressel, D. A. Dickie, C. W. Machan, ACS Catal. 2020, 10, 1146–1151; b) Z. Weng, Y. Wu, M. Wang, J. Jiang, K. Yang, S. Huo, X. F. Wang, Q. Ma, G. W. Brudvig, V. S. Batista, Y. Liang, Z. Feng, H. Wang, Nat. Commun. 2018, 9, 415; c) Y. Wu, J. Jiang, Z. Weng, M. Wang, D. L. J. Broere, Y. Zhong, G. W. Brudvig, Z. Feng, H. Wang, ACS Cent. Sci. 2017, 3, 847–852; d) J. Jiang, A. J. Matula, J. R. Swierk, N. Romano, Y. Wu, V. S. Batista, R. H. Crabtree, J. S. Lindsey, H. Wang, G. W. Brudvig, ACS Catal. 2018, 8, 10131–10136.
- [27] a) M. Abdinejad, A. Seifitokaldani, C. Dao, E. H. Sargent, X.-A. Zhang, H. B. Kraatz, ACS Appl. Energy Mater. 2019, 2, 1330–1335; b) C. G. Margarit, C. Schnedermann, N. G. Asimow, D. G. Nocera, Organometallics 2019, 38, 1219–1223; c) C. Costentin, M. Robert, J. M. Savéant, Acc. Chem. Res. 2015, 48, 2996–3006.

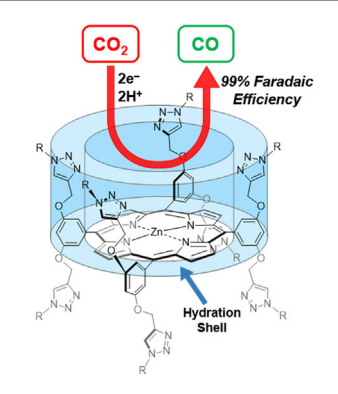
- [28] a) J. S. Lindsey, I. C. Schreiman, H. C. Hsu, P. C. Kearney, A. M. Marguerettaz, J. Org. Chem. 1987, 52, 827–836; b) R. W. Wagner, T. E. Johnson, J. S. Lindsey, Tetrahedron 1997, 53, 6755–6790.
- [29] J. S. Lindsey, Acc. Chem. Res. 2010, 43, 300-311.
- [30] Y. Y. Birdja, J. Shen, M. T. M. Koper, Catal. Today 2017, 288, 37-47.
- [31] E. Haviv, D. Azaiza-Dabbah, R. Carmieli, L. Avram, J. M. L. Martin, R. Neumann, J. Am. Chem. Soc. 2018, 140, 12451 12456.
- [32] C. Costentin, G. Passard, M. Robert, J. M. Savéant, J. Am. Chem. Soc. 2014, 136, 11821 – 11829.
- [33] D. R. Weinberg, C. J. Gagliardi, J. F. Hull, C. F. Murphy, C. A. Kent, B. C. Westlake, A. Paul, D. H. Ess, D. G. McCafferty, T. J. Meyer, *Chem. Rev.* 2012, 112, 4016–4093.
- [34] M. Fathalla, S. C. Li, U. Diebold, A. Alb, J. Jayawickramarajah, Chem. Commun. 2009, 4209 – 4211.
- [35] a) J. E. B. Randles, Trans. Faraday Soc. 1948, 44, 322–327; b) J. E. B. Randles, Trans. Faraday Soc. 1948, 44, 327–338; c) A. Ševčík, Collect. Czech. Chem. Commun. 1948, 13, 349–377.
- [36] B. P. Sullivan, C. M. Bolinger, D. Conrad, W. J. Vining, T. J. Meyer, J. Chem. Soc. Chem. Commun. 1985, 1414–1416.
- [37] A. M. Appel, M. L. Helm, ACS Catal. 2014, 4, 630 633.
- [38] K. T. Ngo, M. McKinnon, B. Mahanti, R. Narayanan, D. C. Grills, M. Z. Ertem, J. Rochford, J. Am. Chem. Soc. 2017, 139, 2604–2618.
- [39] E. S. Rountree, B. D. McCarthy, T. T. Eisenhart, J. L. Dempsey, *Inorg. Chem.* 2014, 53, 9983 – 10002.
- [40] a) Y. Fang, Y. G. Gorbunova, P. Chen, X. Jiang, M. Manowong, A. A. Sinelshchikova, Y. Y. Enakieva, A. G. Martynov, A. Y. Tsivadze, A. Bessmertnykh-Lemeune, C. Stern, R. Guilard, K. M. Kadish, *Inorg. Chem.* 2015, 54, 3501–3512; b) A. G. Maher, M. Liu, D. G. Nocera, *Inorg. Chem.* 2019, 58, 7958–7968.
- [41] a) Y. Hori, H. Wakebe, T. Tsukamoto, O. Koga, *Electrochim. Acta* **1994**, *39*, 1833 1839; b) J. Rosen, G. S. Hutchings, Q. Lu, R. V. Forest, A. Moore, F. Jiao, *ACS Catal.* **2015**, *5*, 4586 4591; c) W. Luo, J. Zhang, M. Li, A. Züttel, *ACS Catal.* **2019**, *9*, 3783 3791.
- [42] G. R. Geier III, J. S. Lindsey, J. Chem. Soc. Perkin Trans. 2 2001, 677 686.
- [43] A. Chapovetsky, M. Welborn, J. M. Luna, R. Haiges, T. F. Miller III, S. C. Marinescu, ACS Cent. Sci. 2018, 4, 397–404.
- [44] G. Chaka, J. L. Sonnenberg, H. B. Schlegel, M. J. Heeg, G. Jaeger, T. J. Nelson, L. A. Ochrymowycz, D. B. Rorabacher, J. Am. Chem. Soc. 2007, 129, 5217–5227.
- [45] I. Azcarate, C. Costentin, M. Robert, J.-M. Savéant, J. Phys. Chem. C 2016, 120, 28951 – 28960.
- [46] M. Wang, K. Torbensen, D. Salvatore, S. Ren, D. Joulie, F. Dumoulin, D. Mendoza, B. Lassalle-Kaiser, U. Isci, C. P. Berlinguette, M. Robert, *Nat. Commun.* 2019, 10, 3602.
- [47] C. Costentin, S. Drouet, M. Robert, J. M. Savéant, J. Am. Chem. Soc. 2012, 134, 11235 – 11242.

Manuscript received: June 10, 2020
Accepted manuscript online: July 23, 2020
Version of record online: ■■ ■■, 0000



## **FULL PAPER**

A set of zinc porphyrin electrocatalysts with flexible triazole units as the second coordination spheres is prepared for cooperative-effect studies. The electrocatalyst with a triazole bundle displays efficient  $CO_2$ -to-CO conversion with a Faradaic efficiency of 99% and a current density of  $-6.2 \text{ mA} \text{ cm}^{-2}$  at -2.4 V vs. Fc/Fc<sup>+</sup>.



## Electrocatalysis

A. Lashgari, C. K. Williams, J. L. Glover, Y. Wu, J. Chai, J. ". Jiang\*



Enhanced Electrocatalytic Activity of a Zinc Porphyrin for CO<sub>2</sub> Reduction:
Cooperative Effects of Triazole Units in the Second Coordination Sphere